Journal of Molecular Catalysis A: Chemical 395 (2014) 128–136

Contents lists available at ScienceDirect

Journal of Molecular Catalysis A: Chemical

journal homepage: www.elsevier.com/locate/molcata

Hydrotalcite-supported gold catalysts for a selective aerobic oxidation of benzyl alcohol driven by visible light

Jing Yu, Jingyi Li*, Huili Wei, Jianwei Zheng, Haiquan Su, Xiaojing Wang

College of Chemistry and Chemical Engineering, Inner Mongolia University, Hohhot, Inner Mongolia 010021, People's Republic of China

ARTICLE INFO

Article history:
Received 22 April 2014
Received in revised form 8 August 2014
Accepted 11 August 2014
Available online 22 August 2014

Keywords:
Gold
Nanoparticles
Hydrotalcite
Photooxidation
Benzyl alcohol

ABSTRACT

Hydrotalcite-supported gold nanoparticles are studied as photocatalysts for the aerobic oxidation of benzyl alcohol and its derivatives without additional base under irradiation by visible light. The effects of the solvent, the hydrotalcite constitution and the gold content on the catalytic reaction are studied. The reactions utilizing benzotrifluoride as the solvent yield the best results. When varying the gold content and support, 2 wt% Au/HT-3 exhibits good catalytic activity. Furthermore, the rate of conversion under visible light is far superior to that in the dark. The catalytic activity can be tuned by manipulating the intensity or wavelength of the light. A reaction mechanism is proposed to rationalize these results: the primary reason for the lower activity observed on recycled catalysts is that the basic sites of hydrotalcite are decreased during the reaction in light.

1. Introduction

Using catalysts can enable access to mild and environmentally friendly conditions. Currently, researchers are focused on metal nanoparticles, particularly the catalytic activity of supported gold nanoparticles. Supported gold nanoparticles have been found to catalyze many reactions, such as C—C couplings [1], the reduction of nitrobenzene [2], the oxidation of organic contaminants [3], phenol hydrogenation to form cyclohexanone [4], the isomerization of epoxides to form allylic alcohols [5] and the esterification of alcohols [6]. Gold nanoparticles have a localized surface plasmon resonance effect (LSPR) [7] under visible light irradiation. The LSPR effect is the collective oscillation of conduction electrons of gold nanoparticles, which resonate with the electromagnetic field of the incident light, so forming high-energy electrons on the gold surface. These high-energy electrons can offer energy to the reaction system, so gold nanoparticles can absorb light energy, and make it into their internal energy [8], which can make the reactant across the reaction barrier. Consequently, sunlight can be utilized.

Hydrotalcite (HT : $[M^{2+}_{1-x}M^{3+}_{x}(OH)]^{x+}[A^{n-}]_{x/n}\cdot yH_2O$) is an interesting inorganic layered building block material that contains metallic hydroxide layers with interlayered anions to balance the positive charges [9]. The metallic cations are in brucite-like sheets, while the anions in the interlayer are flexible and diverse [10]. Acidic and basic sites exist on hydrotalcite, and these sites can play crucial roles during reactions [11]. Moreover, the structure of the most common hydrotalcite is $Mg_6Al_2(OH)_{16}CO_3\cdot nH_2O$.

The dehydrogenation of benzyl alcohol is a representative photocatalytic reaction [12], and the various factors that affect the activity of the catalysts have been studied. Different carriers, such as TiO_2 [13], Al_2O_3 [14], zeolite [15], MOFs [16], MCFs [17] and different metals (such as Au [18], Pd [19], Ag [20], Au–Pd [21], Au–Pt [22], Au–Ag [23], Cu [24]) have been examined. Different catalytic conditions [25] and mechanisms [26] have also been assessed. However, despite the great effort has been expended, numerous aspects remain unclear.

In this study, gold nanoparticles were loaded onto various supports and used as photocatalysts for the selective aerobic oxidation of benzyl alcohol under mild conditions. Adding base is not necessary in this reaction. Usually, base is required in reactions over supported gold catalysts because the bases activate the hydroxyl group on the alcohols [27]. In our study, benzyl alcohol was converted into benzaldehyde with a high selectivity after 24 h under irradiation by visible light. Meanwhile, almost no reaction occurred in the dark under the same conditions. To confirm that the reaction is light-promoted, the light intensity and wavelength were varied. A possible reaction mechanism based on the experimental results was proposed.

* Corresponding author. Tel.: +86 471 4995411; fax: +86 471 4992981.
E-mail address: lijingyicn@163.com (J. Li).

http://dx.doi.org/10.1016/j.molcata.2014.08.023
1381-1169/

2. Experimental

2.1. Preparation of HT

The hydrotalcite supports (HT-*x*, *x*: Mg/Al mole rations, and *x* = 1, 2, 3 and 4) were prepared using a co-precipitation method. (1) A certain ratio of $MgCl_2{\cdot}6H_2O$ and $AlCl_3{\cdot}6H_2O$ was dissolved in redistilled water (1 L) under stirring. (2) NaOH and $Na_2CO_3{\cdot}10H_2O$ were dissolved in redistilled water (4 L). (3) The solution formed in (1) was added drop-wise into the solution formed in (2) with vigorous stirring over approximately 30 min. (4) The mixed suspension was centrifuged and a white solid was obtained. Subsequently the solid was washed six times with Na_2CO_3 (0.1 mol L^{-1}). (5) The wet cake was dried at 80 °C for 20 h in an oven [28].

2.2. Preparation of Au/HT-x catalyst

The 2 wt% Au/HT-3 catalysts were prepared using a sequential deposition/reduction approach. HT-3 (2.5 g) was dispersed in redistilled water (50 mL) and sonicated for 10 min. The pH of the solution was adjusted to 10 using NaOH (0.5 mol L^{-1}) with stirring. Afterward, the $HAuCl_4$ solution was added dropwise under sonication. Subsequently, lysine (20 mL) was added to the mixture. After stirring for 30 min, a fresh $NaBH_4$ solution was added. This slurry was filtered before being washed with deionized water and ethanol, respectively. The resulting mixture was dried at 60 °C for 12 h. The other catalysts, including 2 wt% Au/HT-*x* (*x* = 1, 2 and 4), *y* wt% Au/HT-3 (*y*: 0.5, 1, 2 and 3, respectively), 2 wt% Au/γ-Al_2O_3 and 2 wt% Au/$Mg(OH)_2$ were prepared using the same method [28].

2.3. Recycling use of catalyst

Method 1: Firstly, catalyst and reactant were separated via centrifugation. Afterward, the catalyst was washed with deionized water and ethanol. Finally, the catalyst was dried at 60 °C for 12 h. The recycled catalyst was reused in the next run under the same conditions [29].

Method 2: Firstly, catalyst and reactant were separated via centrifugation. Afterward, the catalyst was washed with Na_2CO_3 (0.1 mol L^{-1}) and ethanol. Finally, the catalyst was dried at 60 °C for 12 h. The recycled catalyst was reused in the next run under the same conditions.

2.4. Catalyst characterization

The X-ray diffraction patterns (XRD) of the samples were recorded on a RIGAKU D/MAX-2500 X-ray diffractometer using CuKα radiation (λ = 1.5405 Å) at 40 kV and 100 mA. The diffraction data were collected from 5° to 80°. The gold contents of the samples were quantitated using atomic absorption spectroscopy (AAS) on a GBC AVANTA YX-05 instrument. The X-ray photoelectron spectroscopy (XPS) measurements were performed on a Kratos XSAM800 using AlKα radiation. The binding energy was calibrated using the C1s photoelectron peak at 284.8 eV as a reference. The particle sizes and morphologies of the samples were determined using transmission electron micrographs (TEM) taken on a FEI Tecnai G2 F20 S-Twin apparatus with a 200 kV acceleration voltage. UV–visible diffuse reflectance spectra (UV–vis DRS) were detected on U-3900 made by Hitachi. Temperature-programmed desorption of CO_2 (CO_2-TPD) was performed on a Micromeritics AutoChem 2920 II instrument. The product was quantitatively analyzed with a GC-2014C gas chromatograph (GC). The identity of the product was confirmed via gas chromatography–mass spectrometry (GC–MS) on a Finnigan LCQ Advantage MAX instrument.

Table 1
Crystal spacing of HT-x.

Entry	Catalysts	*d* value (nm)
1	HT-1	0.772
2	HT-2	0.783
3	HT-3	0.787
4	HT-4	0.796

2.5. Catalytic test: aerobic oxidation of benzyl alcohol

The reaction was carried out in a batch-type reaction with stirring. Typically, the catalyst powder (50 mg), benzyl alcohol (2 mmol) and solvent (10 mL) were placed in a 50 mL round-bottom flask; a LED lamp (200 W, 400–800 nm) was used as a light source. The system was filled with pure oxygen and sealed. A small amount of reactant was separated at regular intervals and quantitatively analyzed by GC. Afterward, the products were identified with a GC–MS spectrometer. For comparison, the reaction was performed simultaneously in the dark under the same conditions [30].

2.6. Hydrogen peroxide test

This kind of examination method is put forward by H. Bader et al. in 1988 [31]. The particular way is shown as follows: the sample (9 mL) after 24 h was placed in a 50 mL round-bottom flask. The buffer solution (pH = 6, 1 mL) was added to achieve pH 6 in the final solution with stirring. Then DPD reagent (N,N-diethyl-1,4-phenylenediammonium sulphate, 17 μL) and POD reagent (peroxidase product from horseradish, 17 μL) were added in the solution [31].

3. Results and discussion

3.1. Catalysts characterization

The structures of various supports and catalysts are confirmed by XRD analysis. Fig. 1A shows the XRD patterns of the supports, including γ-Al_2O_3, MgO and hydrotalcite with various Mg/Al ratios (HT-*x*, *x* stands for Mg/Al mole rations, *x* = 1, 2, 3 and 4), and revealing a series of characteristic patterns of inorganic structures. Fig. 1A (c–f) shows a series of characteristic patterns for the hydrotalcite structure. The diffraction peaks could be indexed to a pure hexagonal phase of hydrotalcites, especially the characteristic reflections (0 0 3) that exhibit a high intensity and a narrow line width [28]. The lattice parameters of HT-3 are $a = 3.058 \pm 0.004$ Å, $c = 23.969 \pm 0.062$ Å, $\alpha = 90°$, $\beta = 90°$, $\gamma = 120°$, and $V = 190.47$ Å^3. Fig. 1B is the local amplification of Fig. 1A from 5° to 30°, and blue shifts of these peaks appear when increasing the Mg/Al ratio. The inter-planar crystal spacing is measured using the (0 0 3) diffraction peak with the Bragg formula ($2d \sin\theta = n\lambda$). The *d* value increases with the molar proportions of magnesium (Table 1). This phenomenon shows that a lattice expansion makes the XRD peaks move toward a smaller angle. Fig. 1C shows the characteristic peaks of supported samples (Au/γ-Al_2O_3, Au/$Mg(OH)_2$ and Au/HT-*x*) with the same gold content (2 wt%). An XRD pattern almost identical to HT-*x* was obtained for Au/HT-*x*, indicating that the crystal structure of the nano-crystalline support is conserved. Moreover, the characteristic diffraction peaks of the Au nanoparticles can be observed within the patterns. The MgO turned into brucite after the catalyst was prepared; possibly similar to a "memory effect" of hydrotalcite. (Calcined hydrotalcites can be reconstructed back to a layered structure when it is in contact with water and appropriate anions. This property is called retro-topotactical transformation. And it is also known as the "memory effect" [32].). Fig. 1D shows the XRD patterns of Au/HT-3 with different gold contents. The Au diffraction

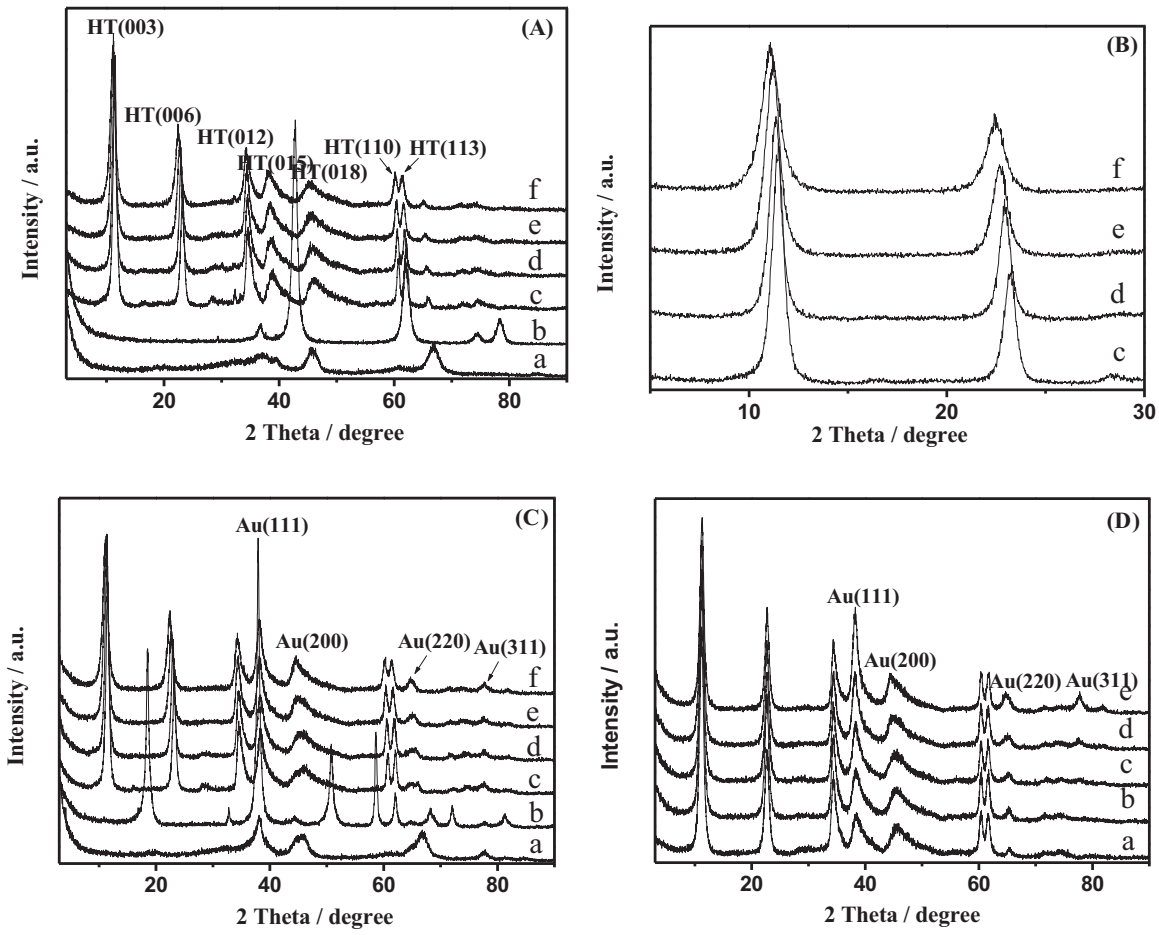

Fig. 1. (A) XRD patterns of the supports: (a) γ-Al_2O_3, (b) MgO, (c) HT-1, (d) HT-2, (e) HT-3, and (f) HT-4. (B) Partially enlarged picture of (A). (C) XRD patterns of the catalysts with various supports: (a) Au/γ-Al_2O_3, (b) Au/$Mg(OH)_2$, (c) Au/HT-1, (d) Au/HT-2, (e) Au/HT-3, and (f) Au/HT-4. (D) XRD patterns of the Au/HT-3 with various gold contents: (a) HT-3, (b) 0.5 wt% Au/HT-3, (c) 1 wt% Au/HT-3, (d) 2 wt% Au/HT-3, (e) 3 wt% Au/HT-3.

peaks intensify when the gold content increases. This phenomenon reveals that the size of the gold nanoparticles increases with the gold content, agreeing with the TEM data. The crystal structure of HT-3 is retained after the gold nanoparticles are deposited.

Fig. 2 shows the corresponding Au 4f XPS spectra of the 2 wt% Au/HT-3. The catalysts clearly contain Au^0. As shown in Fig. 2, the binding energies for the Au $4f_{7/2}$ (83.70 eV) and Au $4f_{5/2}$ (87.35 eV) electrons are observed. The binding energies of these two peaks correspond to the reduced state of gold [12,33]. The higher binding energy (88.90 eV) corresponds to the XPS spectra of Mg 2S.

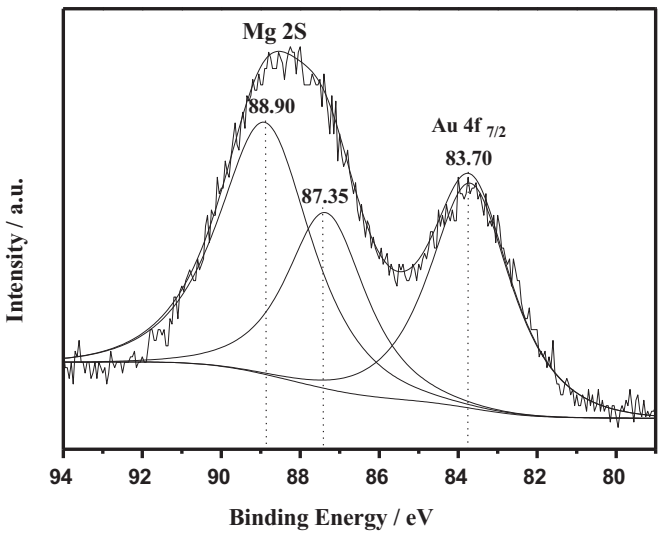

Fig. 2. XPS spectra of the Au 4f core level line for 2 wt% Au/HT-3.

The gold content is analyzed using atomic absorption spectroscopy (AAS), and the results are shown in Table 2. The realistic gold content of the samples is slightly smaller than the theoretical value. Comparing the results of the catalysts (Table 2, entries 3 and 5–9) reveals that the nature of the supports affects the gold content [34].

Table 2
Gold content and nanoparticle size of the supported gold catalysts.

Entry	Catalysts	Au content[a] (wt%)	Mean Au size[b] (nm)
1	0.5 wt% Au/HT-3	0.35	9.28
2	1 wt% Au/HT-3	0.85	11.20
3	2 wt% Au/HT-3	1.96	10.54
4	3 wt% Au/HT-3	2.24	11.66
5	2 wt% Au/HT-1	1.80	10.23
6	2 wt% Au/HT-2	1.82	9.82
7	2 wt% Au/HT-4	1.62	11.84
8	2 wt% Au/γ-Al_2O_3	1.24	10.54
9	2 wt% Au/$Mg(OH)_2$	1.16	11.00
10	2 wt% Au/HT-3	1.31	11.24[c] (10.71)[d]

[a] Measured by AAS.
[b] Obtained from TEM.
[c] The recycled catalyst after light reaction.
[d] The recycled catalyst after dark reaction.

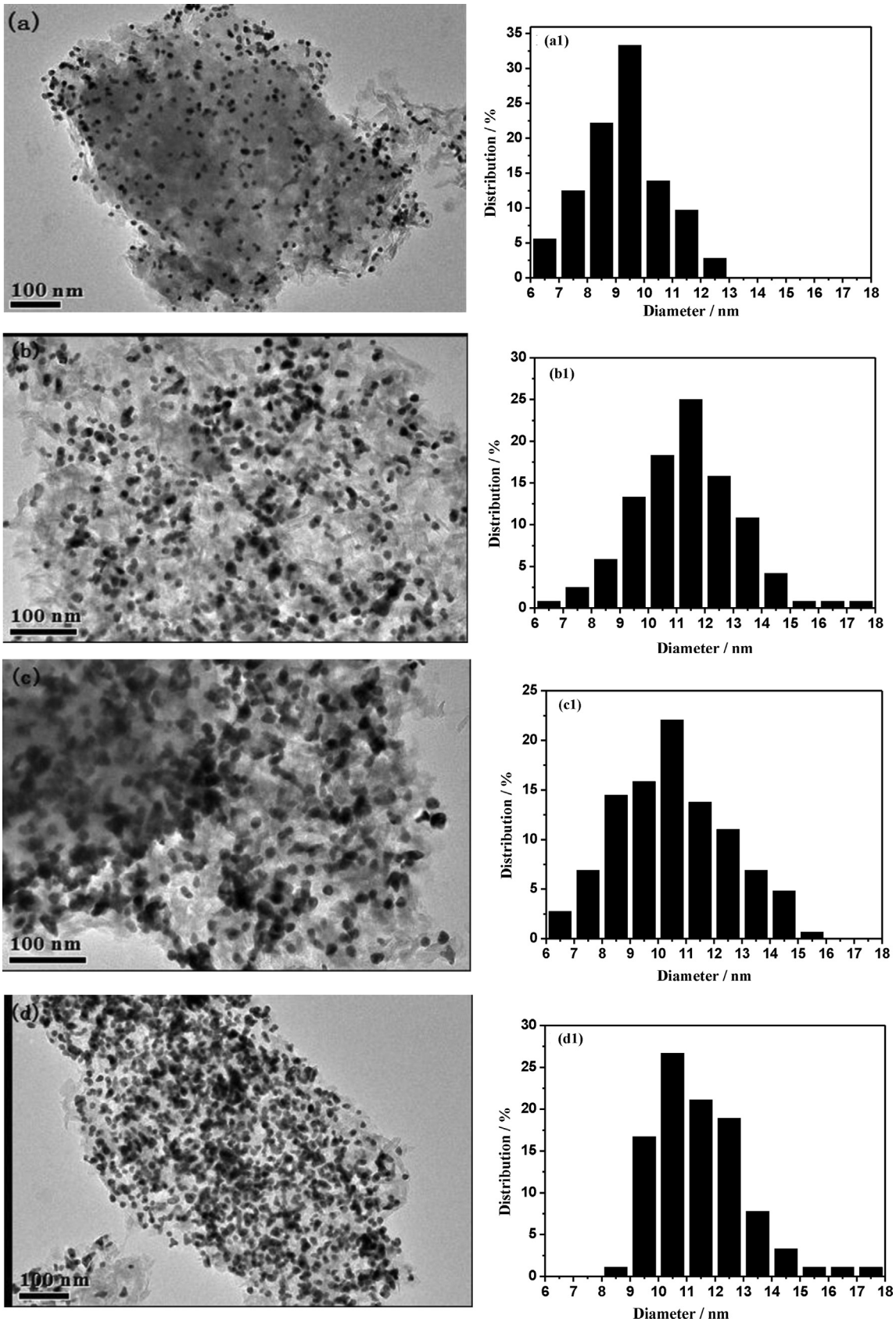

Fig. 3. TEM images of the (a) 0.5 wt% Au/HT-3, (b) 1 wt% Au/HT-3, (c) 2 wt% Au/HT-3, (d) 3 wt% Au/HT-3, (e) recycled 2 wt% Au/HT-3 after irradiation with light, (f) recycled 2 wt% Au/HT-3 after a reaction in the dark, (g) HRTEM images of Au nanoparticles. (a1–f1) Distributions of corresponding particle size.

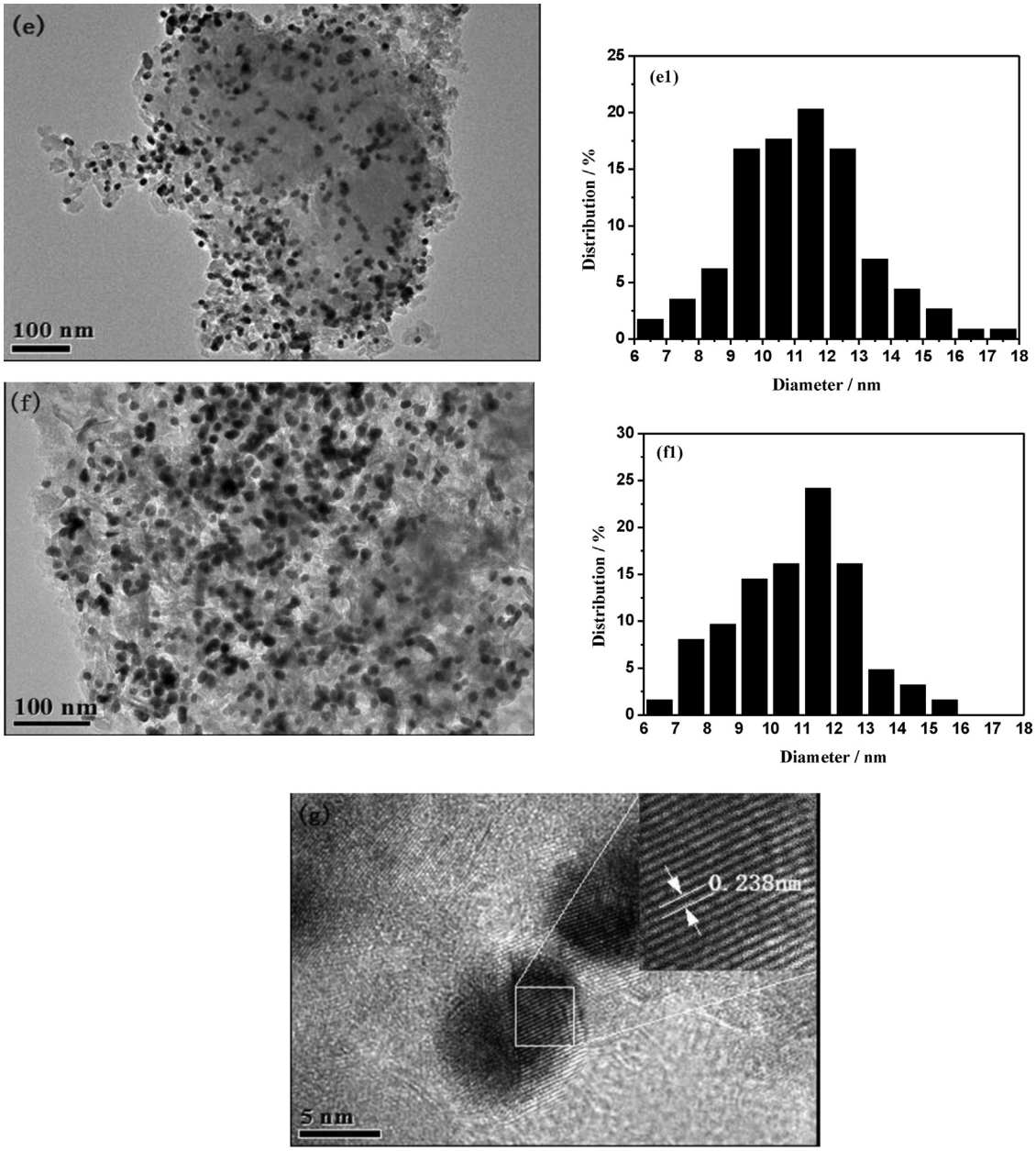

Fig. 3. (*Continued*).

The particle size distribution is determined by TEM, ranging from 8 to 12 nm. The results are given in Table 2 and Fig. 3 and S1. The TEM image shows that the Au nanoparticles are spherical and highly dispersed. The mean diameter of the gold nanoparticles increases slightly after increasing the gold content except for the 1 wt% Au/HT-3 (Table 2, entries 1–4). The high-resolution TEM (HRTEM) images reveal the well-defined crystalline gold nanoparticles and the marked inter-planar spacing is about 0.238 nm that corresponds to the (1 1 1) plane for face-centered cubic gold. Haider and coworkers found that a catalyst with 9 nm Au particles is the most active when aerobically oxidizing 1-phenylethanol over Au/Cu–Mg–Al–O [35].

The UV–visible diffuse reflectance spectra of the catalysts are shown in Fig. 4. An absorption band appears at about 520–530 nm, which is the characteristic SPR absorption band of Au nanoparticles. A red shift of the peak at about 520–530 nm occurs from 0.5 wt% Au/HT-3 to 3 wt% Au/HT-3, which explains the increase of Au particle size (the result is consistent with that of XRD and TEM. It is shown in Fig. 4A).

The basic sites of supports were examined by temperature-programmed desorption (TPD) of CO_2. As shown in Fig. 5, the desorption of CO_2 was observed from HT-*x*, Al_2O_3, and MgO, which indicates that basic sites exist on these supports. From the intensity and area of the CO_2 desorption peak, we can see that HT-*x* possess relatively more basic sites. Only very weak CO_2 desorption peaks could be discerned in the case of Al_2O_3 and MgO, which suggests that these supports have fewer basic sites.

3.2. Activity tests

To determine the optimal reaction conditions, we tested various solvents, supports and gold contents. The 2 wt% Au/HT-3 was initially tested during the photocatalytic aerobic oxidation of benzyl alcohol while using O_2 as the oxidant in different solvents. Of the

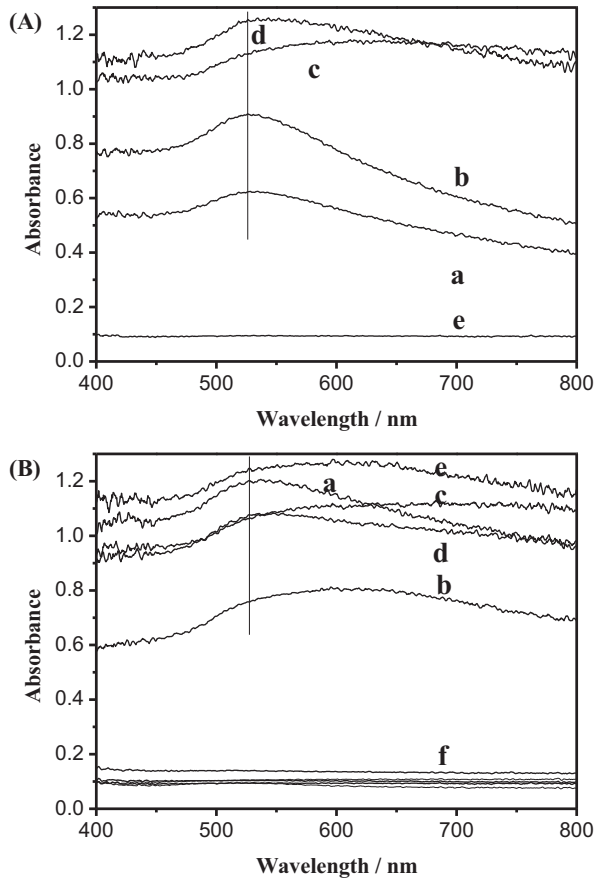

Fig. 4. (A) UV–visible diffuse reflectance spectra of the Au/HT-3 with various gold contents and HT-3: (a) 0.5 wt% Au/HT-3, (b) 1 wt% Au/HT-3, (c) 2 wt% Au/HT-3, (d) 3 wt% Au/HT-3, (e) HT-3. (B) UV–visible diffuse reflectance spectra of the catalysts with different supports and supports: (a) Au/γ-Al_2O_3, (b) Au/Mg$(OH)_2$, (c) Au/HT-1, (d) Au/HT-2, (e) Au/HT-4, and (f) all kinds of supports related with the above catalysts.

solvents tested (Table 3), moderate conversions (more than 40%) of benzyl alcohol with a high selectivity for benzyl aldehyde were obtained when using less polar solvents, such as toluene, mesitylene, benzotrifluoride and 1,4-dioxane; the conversion was the highest (72.93%) when benzotrifluoride was used (Table 3, entries 1–4). In contrast, polar solvents (Table 3, entries 5 and 6) caused a significant drop in conversion because they may compete with the

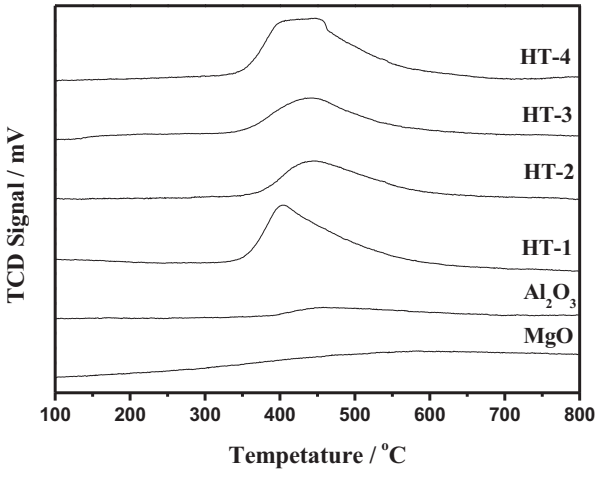

Fig. 5. The CO_2-TPD of different supports.

Table 3
Effect of the solvent on the aerobic oxidation of benzyl alcohol over 2 wt% Au/HT-3.[a]

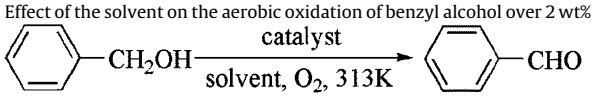

Entry	Solvent	In visible light[b]		In the dark[b]	
		Conv. (%)	Sel. (%)	Conv. (%)	Sel. (%)
1	Toluene	42.8	97.58	5.76	>99
2	Mesitylene	49.55	>99	29.26	>99
3	Benzotrifluoride	72.93	96.78	3.57	>99
4	1,4-dioxane	56.32	94.92	24.12	93.55
5	DMF	20.68	>99	6.29	>99
6	DMSO	0	0	0	0

[a] *Reaction conditions*: solvent (10 mL), benzyl alcohol (2 mmol), catalyst (50 mg), O_2 (1 atm), exposure time (48 h). Light source: LED lamp. The light intensity between 400 and 800 nm is 1.70 W cm^{-2}. The solution temperature during exposure is 313 K.
[b] Conversion rate and selectivity are determined by GC.

reactants for the catalytic sites. Therefore, we chose to use benzotrifluoride in the later experiments. The conversion under light was far higher than that in dark. Therefore, the catalysts could catalyze the light-induced oxidation of benzyl alcohol.

Subsequently, the effects of the support and gold content were tested. Because of the experimental limitations, a few differences in the gold content and size distribution appeared within the series of catalysts (these catalysts included 2 wt% Au/HT-*x* and *y* wt% Au/HT-3); however, these data were within the allowable error range. The results for the oxidation of benzyl alcohol are summarized in Table 4. No conversion occurred without the catalyst or with only the HT-3 support (Table 4, entries 1 and 2), confirming that the gold nanoparticles are crucial for the reaction system. No reaction occurred without O_2 (Table 4, entry 7). Therefore, oxygen participates in the reaction. Subsequently, the photocatalytic aerobic oxidation of benzyl alcohol was carried out over *y* wt% Au/HT-3 with different gold contents (Table 4, entries 3–6). The conversion rate showed a reversed U-shape when increasing the gold content; 2 wt% Au/HT-3 exhibited the highest conversion (57.53%) for the selective aerobic oxidation of benzyl alcohol. After the radical scavengers TEMPO were added into the reaction system, the conversation under visible light irradiation was greatly improved, but

Table 4
Oxidation of benzyl alcohol over supported gold catalysts.[a]

Entry	Catalysts	In visible light[b]		In the dark[b]	
		Conv. (%)	Sel. (%)	Conv. (%)	Sel. (%)
1	–	0	0	0	0
2	HT-3	0	0	0	0
3	0.5 wt% Au/HT-3	28.32	91.56	1.44	>99
4	1 wt% Au/HT-3	36.01	92.59	2.53	>99
5	2 wt% Au/HT-3	57.53	93.82	4.78	91.47
6	3 wt% Au/HT-3	55.97	94.82	3.77	90.98
7[c]	2 wt% Au/HT-3	0	0	0	0
8	2 wt% Au/HT-1	36.78	94.90	3.17	>99
9	2 wt% Au/HT-2	61.66	93.46	4.91	>99
10	2 wt% Au/HT-4	52.89	91.31	5.20	89.45
11	2 wt% Au/γ-Al_2O_3	7.63	>99	1.30	>99
12	2 wt% Au/Mg$(OH)_2$	6.09	>99	2.17	>99
13[d]	2 wt% Au/HT-3	27.73	91.38	0.97	>99
14[e]	2 wt% Au/HT-3	49.44	94.04	1.86	>99
15[f]	2 wt% Au/HT-3	71.24(<1)[c]	93.19(>99)[c]	1.13	>99

[a] *Reaction conditions*: benzotrifluoride (10 mL), benzyl alcohol (2 mmol), catalyst (50 mg), O_2 (1 atm), exposure time (24 h). Light source: LED lamp. The light intensity between 400 and 800 nm is 1.70 W cm^{-2}. The solution temperature during exposure is 313 K.
[b] Conversion rate and selectivity are determined by GC.
[c] The reaction is carried out under Ar.
[d] The reusing of the catalyst by method 1 for the second time after light reaction.
[e] The reusing of the catalyst by method 2 for the second time after light reaction.
[f] TEMPO (0.042 mmol) was added into the reaction system.

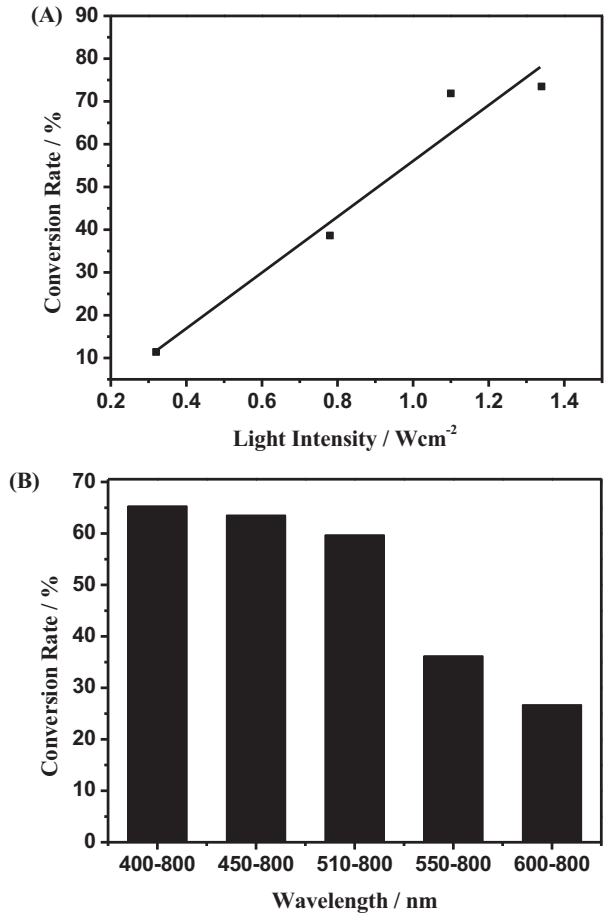

Fig. 6. (A) Effect of light intensity on the photooxidation of benzyl alcohol. (B) Effect of the range of light wavelengths on the photooxidation of benzyl alcohol.

it had no effect on the reaction in dark. And it is worth noting that no reaction occurred in Ar atmosphere even after the addition of TEMPO. Therefore, it suggests that light and O_2 are essential factors in the reaction process (Table 4, entry 15).

For comparison, catalysts with different supports and the same gold content (2 wt%) were tested during the aerobic oxidation of benzyl alcohol with O_2 and benzotrifluoride. The 2 wt% Au/HT-*x* (Table 4, entry 5 and entries 8–10) provided a moderate conversion of benzyl alcohol and a high selectivity for benzaldehyde; benzyl benzoate was obtained as the sole byproduct. Of the various supports tested, a highest catalytic activity was obtained over 2 wt% Au/HT-2 (61.66%). Little conversion proceeded over Au/γ-Al_2O_3 or Au/$Mg(OH)_2$ (Table 4, entries 11 and 12). These inferior activities indicate that the cooperation of magnesium and aluminum is critical for this catalytic reaction.

These experimental results clearly indicate that the 2 wt% Au/HT-3 is a suitable catalyst for the selective light-induced aerobic oxidation of benzyl alcohol. We chose HT-3 as a support because it is the most common hydrotalcite structure. In addition, the cooperative interaction between the gold and the support is essential.

3.3. Effect of light intensity and light wavelength

To verify that the catalytic reaction is light-promoted, the effects of the light intensity and wavelength were studied. The conversion of benzyl alcohol over 2 wt% Au/HT-3 increased gradually when the light intensified. The different light intensity (including 0.32, 0.78, 1.10, 1.34 W cm^{-1}) was transformed, and the results are shown in Fig. 6A. This trend reveals a strong dependence on the intensity of the light when oxidizing benzyl alcohol. A higher light intensity can provide more energy to Au nanoparticles. Consequently, a higher light intensity benefited the interaction between the Au nanoparticles and the reactants, favoring the formation of Au—H bonds [36], increasing the conversion. Moreover, more oxygen molecules can be activated on the gold nanoparticles, promoting the completion of the catalytic cycle. When using different light wavelengths (including 400–800, 450–800, 510–800, 550–800 and 600–800 nm), the reaction was carried out under identical conditions. The results are summarized in Fig. 6B. The conversion of benzyl alcohol gradually declined as the wavelength increased up to 550 nm; after that point, the conversion rapidly decreased. These results are consistent with the strong absorption of gold nanoparticles at 515–535 nm [37]. Therefore, the above results indicate that the catalytic reaction is light-promoted.

3.4. Oxidation of various alcohols

Subsequently, the reaction was extended to benzyl alcohol derivatives and aliphatic alcohols under the same reaction conditions, generating the corresponding aldehydes or ketones with a high selectivity. The results are summarized in Table 5. The benzyl alcohol derivatives containing electron-donating groups (Table 5, entries 2 and 3) are oxidized more easily than those with electron-withdrawing groups (Table 5, entry 4). Furthermore, the oxidization of secondary alcohols, such as 1-phenyl ethanol, occurred with a high conversion (90.13%, Table 5, entry 5). The aerobic oxidation of allylic alcohols, such as cinnamyl alcohol and crotyl alcohol (Table 5, entries 6 and 7) also proceeded efficiently over 2 wt% Au/HT-3 (47.65% and 54.85% conversion, respectively) with a high selectivity (>99% and 79.87%, respectively). Meanwhile, this catalyst can convert hetero-aromatic alcohols, such as furfuryl alcohol and pyridine methanol (Table 5, entries 8 and 9), to their corresponding aldehydes with high conversions (77.12% and 66.23%, respectively). In addition, catalytic activity was apparent even for aliphatic alcohols, such as 1-octanol and 2-octanol (Table 5, entries 10 and 11). The conversion of most of the light-promoted reactions was 20 times greater than that in the dark, demonstrating that the gold materials are photocatalysts.

3.5. Reaction mechanism

Based on the experimental results, a reaction pathway was proposed for this oxidation. A possible mechanism for the photocatalytic aerobic oxidation of benzyl alcohol over Au/HT-3 is presented in Scheme 1 [38–44]. The first step of the reaction is adsorption of benzyl alcohol on the hydrotalcite supports. Subsequently, the Brønsted-basic sites on the hydrotalcite facilitate β-hydrogen atom elimination, generating a water molecule and forming the metal–alkoxide intermediate. Under visible light irradiation, gold nanoparticles activated oxygen molecules due to the LSPR effect [45,46]. Afterward, the hydrogen atom on the α-carbon of the benzyl alcohol was passed onto the Au nanoparticles, forming an adsorbed peroxide species (Au—O—O—H) and the selective oxidation product benzaldehyde. This species reacts with hydrogen atom on the α-carbon of another benzyl alcohol to form adsorbed hydrogen peroxide (Au—HOOH), hydrogen peroxide were detected in the reaction by the test of hydrogen peroxide. Finally, the H_2O_2 can decompose (E_a = 0.17 eV) or desorb (E_a = 0.19 eV) from the gold nanoparticles. The support is partially restored to its initial state, and the reaction cycle is completed. Seven key elementary steps in the reaction are shown as follows:

$$PhCH_2OH + OH^-(HT\text{-}3) \rightarrow PhCH_2O\text{-}HT\text{-}3 + H_2O \quad (1)$$

$$Au* + O_2 \rightarrow Au—O—O \quad (2)$$

Table 5
Oxidation of different alcohols over 2 wt% Au/HT-3.[a]

Entry	Substrate	Target product	In visible light[b]		In the dark[b]	
			Conv. (%)	Sel. (%)	Conv. (%)	Sel. (%)
1	Benzyl alcohol	Benzyl aldehyde	57.41	93.82	3.68	91.47
2	4-Methylbenzyl alcohol	4-Methylbenzyl aldehyde	57.25	>99	2.87	>99
3	4-Methoxybenzyl alcohol	4-Methoxybenzyl aldehyde	60.73	>99	8.94	>99
4	4-Chlorobenzyl alcohol	4-Chlorobenzyl aldehyde	29.98	>99	2.30	>99
5	1-Phenyl ethanol	Acetophenone	90.13	>99	1.69	>99
6	Cinnamyl alcohol	Cinnamyl aldehyde	47.65	>99	2.31	83.74
7[c]	Crotyl alcohol	Crotonaldehyde	54.85	79.87	3.12	94.95
8[d]	Furfuryl alcohol	Furfuryl aldehyde	77.12	25.23	2.84	99.72
9[d]	Pyridine methanol	Pyridine formaldehyde	66.23	69.09	14.39	81.38
10[d]	1-Octanol	Octanal	10.74	>99	2.37	>99
11[d]	2-Octanol	2-Octanone	10.13	>99	0	>99

[a] *Reaction conditions*: benzotrifluoride (10 mL), alcohol (2 mmol), catalyst (50 mg), O_2 (1 atm), exposure time (24 h). Light source: LED lamp. The light intensity between 400 and 800 nm is 1.70 W cm^{-2}. The solution temperature during exposure is 313 K.
[b] Conversion rate is determined by GC.
[c] *Reaction conditions*: 1,4-dioxane (10 mL), alcohol (2 mmol), catalyst (50 mg), O_2 (1 atm), exposure time (22 h). Light source: LED lamp. The light intensity between 400 and 800 nm is 1.70 W cm^{-2}. The solution temperature during exposure is 313 K.
[d] *Reaction conditions*: 1,4-dioxane (10 mL), alcohol (2 mmol), catalyst (50 mg), O_2 (1 atm), exposure time (46 h). Light source: LED lamp. The light intensity between 400 and 800 nm is 1.70 W cm^{-2}. The solution temperature during exposure is 313 K.

$$PhCH_2O\text{-}HT\text{-}3 + Au{-}O{-}O + h\nu \rightarrow Au{-}O{-}O{-}H \quad (3)$$

$$Au{-}O{-}O{-}H + PhCH_2O\text{-}HT\text{-}3 \rightarrow Au{-}H{-}O{-}O{-}H + PhCHO + e^{-}(HT\text{-}3) \quad (4)$$

$$Au{-}H{-}O{-}O{-}H \rightarrow 2OH + Au* \quad (5)$$

$$HO + e^{-}(HT\text{-}3) \rightarrow OH^{-}(HT\text{-}3) \quad (6)$$

$$Au{-}H{-}O{-}O{-}H \rightarrow H_2O_2(sol) + Au* \quad (7)$$

We also found that the catalytic activity of the recycled catalyst after washed by water is obviously decreased (Table 4, entry 13). Some researchers have suggested three reasons for this decrease in catalytic activity: (1) the gold nanoparticles fall off the support [47], (2) the gold nanoparticles agglomerate [48] or (3) the organic reactants can poison the catalyst [49]. To identify the major factor, the recovered catalyst was characterized. The AAS results show that gold nanoparticles fall off the support after recycling, leaving a gold content of 1.31 wt% (Table 2, entry 10), which is between 1 wt% and 2 wt%. According to the effects of the gold content on the catalytic efficiency, the conversion rate when using the recycled catalyst should be between 36.01% and 57.53% (Table 4, entry 4 and

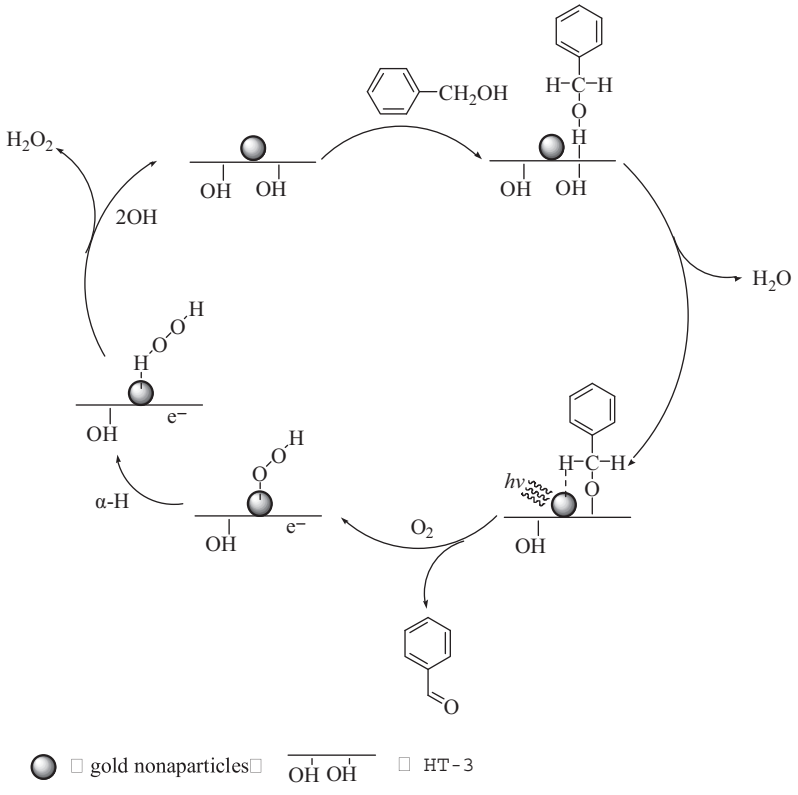

Scheme 1. The mechanism for the photo-catalyzed aerobic oxidations of benzyl alcohol on 2 wt% Au/HT-3.

5). However, the conversion is actually 27.73%, falling outside of the theoretical range (Table 4, entry 13). But the conversion returned to 49.44% after the catalysts was washed with Na_2CO_3, which showed the basic sites of the support had an effect on the catalytic activity. This phenomenon suggested that the basic site was reduced during the reaction (Table 4, entry 14). The TEM image of the recycled catalyst indicates that the mean diameter of the gold nanoparticles is similar to that of the originals (Table 2, entries 3 and 10), suggesting that the gold nanoparticles have not agglomerated. We also propose that no organic reactants are adsorbed on the catalyst surface after washing and drying the catalyst, no poisoning occurs.

According to the mechanism, the desorption of H_2O_2 decreases the Brønsted-base sites on the HT during the reaction, explaining the decrease in conversion over the recycled catalyst. The formation of molecular H_2O_2 consumes two hydrogens from two benzyl alcohol molecules are involved in the reaction. This process will consume two hydroxyl groups on the hydrotalcite. However, only some of the H_2O_2 is decomposed into hydroxylate and returned to the hydrotalcite. Consequently, the Brønsted-basic sites on the HT decrease after catalytic cycle. The reactivity declines as the reaction sites decrease. Meanwhile, the nature of the support will also affect the loading sites of the gold nanoparticles, so gold content of the recycled catalyst is lower than the initial one. In a word, the lower activity of the recycled catalyst is due to the decrease of Brønsted-basic sites on the HT, which reduce the catalytic sites and gold content.

4. Conclusion

These heterogeneous catalysts can photocatalyze the aerobic oxidation of benzyl alcohol and its derivatives. The reaction proceeds with good conversion and selectivity. Using non-polar solvents is beneficial for this oxidation reaction. The gold content of Au/HT-3 and the nature of the supports strongly influence activity. The light intensity and wavelength experiments validate the ability of the catalysts to photocatalyze the oxidation of benzyl alcohol. A possible reaction mechanism is proposed. And this mechanism explains the reduction of catalytic activity when reusing it reasonably.

Acknowledgements

This work was financially supported by NSFC (Nos. 20567002 and 21067007), as well as by the Scientific Research Startup Fund of Inner Mongolia University (203044), the Education Department of Inner Mongolia Autonomous Region (NJ04093), Chunhui Plan of the Education Ministry (Z2004-2-15030 and Z2009-1-01005), the Natural Science Fund of Inner Mongolia (2010MS0203 and 2014MS0201), “513 talents” Plan of Inner Mongolia University and 2013 Annual Grassland Talents Project of Inner Mongolia Autonomous Region.

References

[1] B.Z. Yuan, Y.Y. Pan, Y.W. Li, B.L. Yin, H.F. Jiang, Angew. Chem. Int. Ed. 49 (2010) 4054–4058.
[2] H.Y. Zhu, X.B. Ke, X.Z. Yang, S. Sarina, H.W. Liu, Angew. Chem. Int. Ed. 49 (2010) 9657–9661.
[3] X. Chen, H.Y. Zhu, J.C. Zhao, Z.F. Zheng, X.P. Gao, Angew. Chem. Int. Ed. 47 (2008) 5353–5356.
[4] H.Z. Liu, T. Jiang, B.X. Han, S.G. Liang, Y.X. Zhou, Science 326 (2009) 1250–1252.
[5] C. Raptis, H. Garcia, M. Stratakis, Angew. Chem. Int. Ed. 48 (2009) 3133–3136.
[6] F.Z. Su, J. Ni, H. Sun, Y. Cao, H.Y. He, K.N. Fan, Chem. Eur. J. 14 (2008) 7131–7135.
[7] X. Chen, Z.F. Zheng, X.B. Ke, E. Jaatinen, T.F. Xie, D.J. Wang, C. Guo, J.C. Zhao, H.Y. Zhu, Green Chem. 12 (2010) 414–419.
[8] X.B. Ke, S. Sarina, J. Zhao, X.G. Zhang, J. Chang, H.Y. Zhu, Chem. Commun. 48 (2012) 3509–3511.
[9] O. Meyer, F. Roessner, R.A. Rakoczy, R.W. Fischer, ChemCatChem 2 (2010) 314–321.
[10] S. Abelló, F. Medina, D. Tichit, J. Pérez-Ramírez, J.C. Groen, J.E. Sueiras, P. Salagre, Y. Cesteros, Chem. Eur. J. 11 (2005) 728–739.
[11] Y. Kwon, S.C.S. Lai, P. Rodriguez, M.T.M. Koper, J. Am. Chem. Soc. 133 (2011) 6914–6917.
[12] W.H. Fang, J.S. Chen, Q.H. Zhang, W.P. Deng, Y. Wang, Chem. Eur. J. 17 (2011) 1247–1256.
[13] K. Kimura, S. Naya, Y. Jin-nouchi, H. Tada, J. Phys. Chem. C 116 (2012) 7111–7117.
[14] X.M. Wang, G.J. Wu, N.J. Guan, L.D. Li, Appl. Catal. B 115–116 (2012) 7–15.
[15] X.G. Zhang, X.B. Ke, H.Y. Zhu, Chem. Eur. J. 18 (2012) 8048–8056.
[16] G.Z. Chen, S.J. Wu, H.L. Liu, H.F. Jiang, Y.W. Li, Green Chem. 15 (2013) 230–235.
[17] E.V. Johnston, O. Verho, M.D. Kärkäs, M. Shakeri, C.W. Tai, P. Palmgren, K. Eriksson, S. Oscarsson, J.E. Bäckvall, Chem. Eur. J. 18 (2012) 12202–12206.
[18] Y. Yuan, N. Yan, P.J. Dyson, Inorg. Chem. 50 (2011) 11069–11074.
[19] T. Nishimura, N. Kakiuchi, M. Inoue, S. Uemura, Chem. Commun. (2000) 1245–1246.
[20] T. Mitsudome, Y. Mikami, H. Funai, T. Mizugaki, K. Jitsukawa, K. Kaneda, Angew. Chem. Int. Ed. 47 (2008) 138–141.
[21] L. Wang, W. Zhang, S.J. Zeng, D.S. Su, X.J. Meng, F.S. Xiao, Chin. J. Chem. 30 (2012) 2189–2197.
[22] K. Kaizuka, H. Miyamura, S. Kobayashi, J. Am. Chem. Soc. 132 (2010) 15096–15098.
[23] X.M. Huang, X.G. Wang, X.S. Wang, X.X. Wang, M.W. Tan, W.Z. Ding, X.G. Lu, J. Catal. 301 (2013) 217–226.
[24] M. Dixit, M. Mishra, P.A. Joshi, D.O. Shah, J. Ind. Eng. Chem. 19 (2013) 458–468.
[25] N. Kakiuchi, Y. Maeda, T. Nishimura, S. Uemura, J. Org. Chem. 66 (2001) 6620–6625.
[26] T. Kawabata, Y. Shinozuka, Y. Ohishi, T. Shishido, K. Takaki, K. Takehira, J. Mol. Catal. A 236 (2005) 206–215.
[27] N. Dimitratos, J.A. Lopez-Sanchez, G.J. Hutchings, Chem. Sci. 3 (2012) 20–44.
[28] P. Liu, C. Li, E.J.M. Hensen, Chem. Eur. J. 18 (2012) 12122–12129.
[29] F.Z. Su, Y.M. Liu, L.C. Wang, Y. Cao, H.Y. He, K.N. Fan, Angew. Chem. Int. Ed. 47 (2008) 334–337.
[30] S. Sarina, H.Y. Zhu, E. Jaatinen, Q. Xiao, H.W. Liu, J.F. Jia, C. Chen, J. Zhao, J. Am. Chem. Soc. 135 (2013) 5793–5801.
[31] H. Bader, V. Sturzenegger, J. Hoigné, Water Res. 22 (1988) 1109–1115.
[32] D.P. Debecker, E.M. Gaigneaux, G. Busca, Chem. Eur. J. 15 (2009) 3920–3935.
[33] J. Han, Y. Liu, R. Guo, J. Am. Chem. Soc. 131 (2009) 2016–2026.
[34] T. Chen, F.Z. Zhang, Y. Zhu, Catal. Lett. 143 (2013) 206–218.
[35] P. Haider, J.D. Grunwaldt, A. Baiker, Catal. Today 141 (2009) 349–354.
[36] M. Conte, H. Miyamura, S. Kobayashi, V. Chechik, J. Am. Chem. Soc. 131 (2009) 7189–7196.
[37] H.Y. Zhu, X. Chen, Z.F. Zheng, X.B. Ke, E. Jaatinen, J.C. Zhao, C. Guo, T.F. Xie, D.J. Wang, Chem. Commun. (2009) 7524–7526.
[38] B.N. Zope, D.D. Hibbitts, M. Neurock, R.J. Davis, Science 330 (2010) 74–78.
[39] S. Gowrisankar, H. Neumann, M. Beller, Angew. Chem. Int. Ed. 50 (2011) 5139–5143.
[40] M. Zhang, Q. Wang, C.C. Chen, L. Zang, W.H. Ma, J.C. Zhao, Angew. Chem. Int. Ed. 48 (2009) 6081–6084.
[41] D. Tsukamoto, Y. Shiraishi, Y. Sugano, S. Ichikawa, S. Tanaka, T. Hirai, J. Am. Chem. Soc. 134 (2012) 6309–6315.
[42] K. Shimizu, K. Sugino, K. Sawabe, A. Satsuma, Chem. Eur. J. 15 (2009) 2341–2351.
[43] C. Shang, Z.P. Liu, J. Am. Chem. Soc. 133 (2011) 9938–9947.
[44] D. Tongsakul, S. Nishimura, C. Thammacharoen, S. Ekgasit, K. Ebitani, Ind. Eng. Chem. Res. 51 (2012) 16182–16187.
[45] A. Wittstock, V. Zielasek, J. Biener, C.M. Friend, M. Bäumer, Science 327 (2010) 319–322.
[46] X. Deng, B. Min, A. Guloy, J. Am. Chem. Soc. 127 (2005) 9267–9270.
[47] A. Abad, A. Corma, H. García, Chem. Eur. J. 14 (2008) 212–222.
[48] T. Mitsudome, A. Noujima, T. Mizugaki, K. Jitsukawa, K. Kaneda, Adv. Synth. Catal. 351 (2009) 1890–1896.
[49] J.C.F. Rodriguez-Reyes, C.M. Friend, R.J. Madix, Surf. Sci. 606 (2012) 1129–1134.